Polymer 53 (2012) 4002–4009

Contents lists available at SciVerse ScienceDirect

Polymer

journal homepage: www.elsevier.com/locate/polymer

Enthalpy recovery and structural relaxation in layered glassy polymer films

Thomas M. Murphy [a], D.S. Langhe [b], M. Ponting [b], E. Baer [b], B.D. Freeman [a], D.R. Paul [a,*]

[a] Department of Chemical Engineering and Texas Materials Institute, The University of Texas at Austin, Austin, TX 78712, United States
[b] Department of Macromolecular Science and Engineering, Case Western Reserve University, Cleveland, OH 44106, United States

ARTICLE INFO

Article history:
Received 29 May 2012
Received in revised form
3 July 2012
Accepted 8 July 2012
Available online 16 July 2012

Keywords:
Physical aging
Enthalpy relaxation
Confinement

ABSTRACT

Recent studies of physical aging in confined polymer glasses have revealed that aging behavior in confinement often differs from bulk behavior. This study used DSC to characterize physical aging and structural relaxation in bulk polysulfone (PSF) and co-extruded multilayered films of PSF and an olefin block copolymer (OBC) that have average PSF layer thicknesses of 640 nm, 260 nm, and 185 nm. The films were aged isothermally at 170 °C, and the recovered enthalpy upon reheating was measured over time. The films with 640 nm and 260 nm PSF layers had aging rates very similar to that of bulk PSF, while the film with 185 nm PSF layers had an aging rate slightly greater than the bulk value. The cooling rate dependence of the limiting fictive temperature (T_f') in multilayered and bulk PSF samples was also characterized. Values of T_f' were similar for all films at each cooling rate. The results of this work are in general agreement with our previous gas permeation aging study of multilayered PSF films aged at 35 °C, in which the effect of layer thickness on aging behavior was minimal. This stands in contrast to studies with thin, freestanding PSF films, which exhibit accelerated aging relative to bulk and have aging rates that depend strongly on film thickness.

1. Introduction

Glassy polymers typically exist in a non-equilibrium state in which properties such as specific volume, enthalpy, and entropy are in excess of equilibrium values. Compared to the "rubbery" or "liquid" equilibrium state above the glass transition temperature, T_g, the molecular mobility of the polymer chains is greatly reduced in the glassy state. However, some chain mobility remains, which allows for relaxation of the excess volume as the polymer approaches equilibrium [1]. Fig. 1 shows a simplified view of the enthalpy of a glass-forming polymer as a function of temperature. Upon holding a non-equilibrium glassy polymer at a fixed annealing temperature, T_a, densification will occur over time, and many of the polymer's properties will change. For example, the enthalpy of the sample will decrease. The time-dependent property changes resulting from this densification process are known as physical aging [2]. For glassy engineering thermoplastics at typical service temperatures (i.e., well below T_g), aging is often slow, and equilibrium is practically never achieved on experimentally-accessible timescales [1,2]. The fictive temperature, T_f, is a concept used to characterize the instantaneous state of a glass [3–5]. As indicated in Fig. 1, it is the temperature at which the extrapolated equilibrium line would be intersected by a line drawn through the point representing the current enthalpy value of the sample and having the same slope as that of a sample in the glassy state (i.e., the same heat capacity). If a material is in equilibrium, the fictive temperature and annealing temperature will be the same. For a non-equilibrium glass annealed isothermally below T_g, the fictive temperature will be greater than the annealing temperature, with the difference between the two being a reflection of the departure of the sample's enthalpy from equilibrium. The fictive temperature concept is often used in phenomenological models of structural relaxation and physical aging, such as the Tool-Narayanaswamy-Moynihan (TNM) model, to capture the dependence of the relaxation time on the instantaneous structural state of the polymer [4]. A review by Hodge provides a thorough description of enthalpy relaxation and the models used to describe it [6]. A general review of physical aging (not limited to enthalpy relaxation), written by Hutchinson, also describes enthalpy relaxation studies and theoretical treatments of the aging process [2].

Historically, differential scanning calorimetry (DSC) has been widely used to study physical aging and dynamic structural relaxation (i.e., relaxation that occurs during cooling or heating while the polymer is below T_g) of glassy materials. Early studies by Petrie in the 1970s helped establish DSC as a viable and useful technique for studying physical aging in polymer glasses [7,8]. Much recent work pertaining to physical aging and enthalpy relaxation has

* Corresponding author. Tel.: +1 512 471 5392; fax: +1 512 471 0542.
E-mail address: drp@che.utexas.edu (D.R. Paul).

0032-3861/$ – see front matter © 2012 Elsevier Ltd. All rights reserved.
http://dx.doi.org/10.1016/j.polymer.2012.07.012

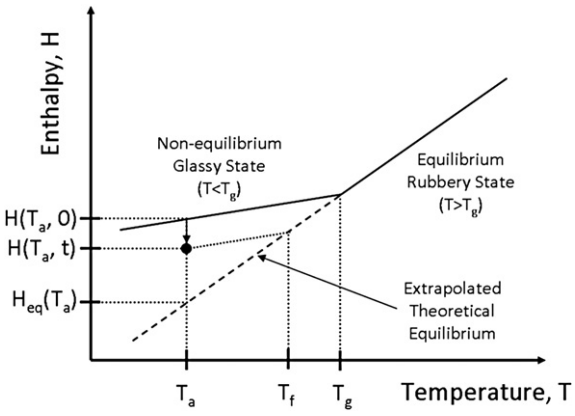

Fig. 1. Qualitative enthalpy vs. temperature diagram for a glass-forming polymer.

focused on aging in confined geometries such as polymer thin films [9], nanocomposites [10–14], and molecular glass-formers confined in nanopores [15].

Koh and Simon used DSC to study the structural relaxation of ultrathin polystyrene (PS) films arranged in stacks [9]. When aged at the same temperature, the ultrathin films (62 nm and 38 nm) required less time to reach equilibrium than bulk films. Thus, physical aging in these thin films was accelerated relative to that in bulk samples. The depressed T_g values in the thin films were cited as the reason for the accelerated aging. When both ultrathin and bulk films were aged at a constant value of $T_g - T_a$ (thus accounting for T_g depression in ultrathin films), rates of aging were similar. The DSC thermograms for the thin films also showed a reduced height in the heat capacity overshoot peak and a broader glass transition relative to those observed in bulk films. Modeling studies indicated that the thinner films had a broader distribution of relaxation times than the corresponding bulk films.

Boucher et al. studied enthalpy recovery in poly(methyl methacrylate) (PMMA)/silica nanocomposites using DSC [12]. Addition of silica nanoparticles did not affect T_g. Physical aging of the nanocomposites was accelerated relative to that of bulk PMMA when aged at 80 °C (i.e., $T_g - 43$ °C). Higher ratios of silica particle surface area to PMMA volume correlated with more rapid physical aging. A recent paper from Cangialosi et al. considered both PMMA-silica and PS-silica nanocomposites and observed accelerated aging in both systems [11]. A decoupling between the segmental mobility (as determined by broadband dielectric spectroscopy) and both the calorimetric T_g and physical aging rate was observed. A model based on the diffusion of free volume holes to the silica/polymer interface was used to rationalize their observations.

Flory et al. investigated the enthalpy relaxation and T_g of nanocomposites of PMMA and both unmodified and amino-functionalized single-wall carbon nanotubes (SWNT) [14]. The T_g of unmodified SWNT nanocomposites was the same as that of pure PMMA, while the amino-functionalized nanocomposites showed a T_g increase of ~17 °C. The physical aging of both nanocomposite systems was reduced relative to that of neat PMMA when aged at the same distance from T_g, as judged by their approach to a constant recovered enthalpy value.

Simon, Park, and McKenna used DSC to study the physical aging of ortho-terphenyl (o-TP) confined in a nanoporous matrix [15]. The confined o-TP exhibited accelerated aging relative to bulk, and the equilibrium state reached by the confined glasses was different from that of the bulk material. Simon et al. were able to model the aging behavior by accounting for isochoric glass formation (i.e., the o-TP "sticks" to the walls of the nanopores and cannot undergo volume changes, thus leading to tensile stresses in the confined o-TP glass).

A study by Langhe et al. explored physical aging of PS layers in multilayered films of PS and polycarbonate (PC) using DSC [16]. The PS/PC films had PS layer thicknesses ranging from 50 to 500 nm. The T_g of the PS layers in these films was independent of layer thickness and essentially the same as that of bulk PS. Isothermal aging studies at 80 °C showed that aging rate decreased as layer thickness decreased. A film with 50 nm PS layers had an aging rate 50% lower than that of bulk PS. The fraction of interphase material (i.e., material surrounding the PS/PC layer interface containing both PS and PC), which increases as layer thickness decreases, was inversely correlated with aging rate. The increased T_g of the interphase material was hypothesized to lead to longer relaxation times, thus reducing the aging rate. It was also suggested that the interphase material could impose mechanical constraints on PS layer relaxation that become more important as the interphase fraction increases. The enthalpy relaxation occurring during cooling these films at different rates was also studied, but the enthalpy recovered upon reheating the sample after cooling did not depend on layer thickness and was similar to that of bulk PS.

Many other recent physical aging studies, using techniques such as gas permeability tracking [17–27], fluorescence spectroscopy [28–31], dielectric spectroscopy [28,32–37], and ellipsometry [38–42], have been aimed at understanding physical aging in confined systems. A concise review of some of these recent studies is provided by Priestley [43]. In most of these studies, the aging behavior of polymers in confinement is different from that of bulk polymers.

Our previous work on physical aging in multilayered polysulfone (PSF) films at 35 °C, which used gas permeability to track physical aging, revealed that the rate of aging in these films is similar to that in bulk films [25]. This work, in which some of the same multilayered film systems from our previous study are used, employs DSC to further explore enthalpy relaxation in these films at temperatures closer to the T_g of PSF.

2. Experimental

2.1. Materials

Polysulfone (UDEL P-3700, Solvay Advanced Polymers) was the primary material of interest in this work. PSF is used as a gas

Table 1
Materials used to produce layered films.

Polymer	Density[a]	T_g	T_m	X_c[b]
UDEL P-3700 Polysulfone (PSF) 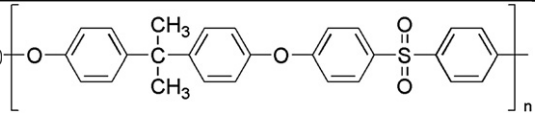	1.24	186 °C	–	–
Infuse 9007 (OBC)	0.866	−60 °C	120 °C	8%

[a] Density values taken from manufacturer data sheets; reported in units of g/cm^3.
[b] Crystallinity determined by DSC and reported in wt.%.

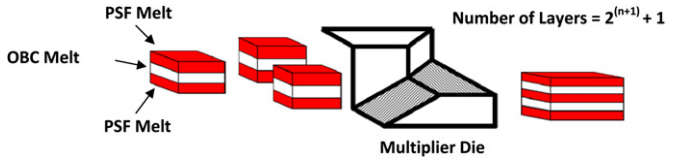

Fig. 2. Schematic illustration of the co-extrusion process used to produce multilayered films [47].

separation membrane material, and many aging studies of this material have focused on the evolution of gas permeability over time in both bulk and freestanding thin films [18,19,21,22,44,45]. Infuse 9007, an olefin block copolymer (OBC) supplied by Dow Chemical Co. was used as the co-layering material in the production of multilayered PSF/OBC films. The PSF has a T_g of ~186 °C, while the OBC material has a T_g of ~ −60 °C. Because the OBC material is not in the glassy state at the aging temperatures used in this study, it does not undergo physical aging. It was chosen because it has relatively low crystallinity (X_c ~ 8 wt.%) and suitable rheological properties at the extrusion temperature to allow for the production of multilayered PSF/OBC films. Table 1 summarizes key properties of the materials used in this study.

2.2. Film production

Multilayered films of PSF and OBC were produced at Case Western Reserve University (CWRU) using a layer-multiplying co-extrusion process. The production of multilayered PSF/OBC films is described in greater detail elsewhere [25], and other publications provide more detail about the production of multilayered films in general [46–48]. The films were produced with a target composition of 50/50 PSF/OBC by volume, so the PSF layer thickness was determined by the number of layer multipliers and the overall feed rate. The multilayered films had 129, 257, or 513 total layers. Bulk films of pure PSF were also produced during the extrusion runs. The extrusion temperature was ~290 °C, which allows for melt state equilibration between PSF and OBC and results in well-adhered layers. Fig. 2 presents the general extrusion scheme used to produce the multilayered films for this study [47].

2.3. Layer thickness and composition characterization of layered films

Atomic force microscopy (AFM) was used to measure the average layer thickness in the multilayered films. The overall thickness of the films was measured using a handheld micrometer. To determine the actual mass percentage of PSF in each sample, which is needed to normalize both the DSC thermograms and the calculated recovered enthalpy, elemental analysis for sulfur was performed by Galbraith Laboratories (Knoxville, TN). Because only the PSF layers contain sulfur and the repeat unit of PSF is known, the mass fraction of PSF in a sample can be readily calculated from the elemental analysis results. The results of elemental analysis showed that the PSF/OBC films all had similar PSF content (~65–66 wt.%), although it was slightly higher than the target composition. This was not unexpected, because the rubbery OBC material, which has a lower viscosity than PSF at the extrusion temperature, tends to flow towards the edges of the film and accumulate there as it exits the coat-hanger die at the end of the extruder. As a result, the film has noticeably thicker edges with more rubbery material there. All samples used for elemental analysis, AFM, and DSC studies and were taken from the center of the film roll. Table 2 summarizes the composition and thickness data for the PSF/OBC films.

Table 2
Thickness and composition data for the films considered in this study.

Sample[a]	Nominal composition (vol.% PSF)	Overall thickness	PSF layer thickness[b]	Mass% PSF	
				Nominal[c]	Elemental analysis[d]
Bulk	100%	76 μm	–	100%	100%
129L	50%	89 μm	640 ± 130 nm	59%	66.3 ± 0.5%
257L	50%	102 μm	260 ± 40 nm	59%	65.3 ± 0.8%
513L	50%	76 μm	185 ± 30 nm	59%	64.7 ± 0.6%

[a] 129L = 129 layer PSF/OBC film, 257L = 257 layer PSF/OBC film, etc.
[b] Average layer thickness ± standard deviation from AFM images.
[c] Calculated from target composition (50/50) and densities of PSF and OBC.
[d] Determined by elemental analysis for sulfur.

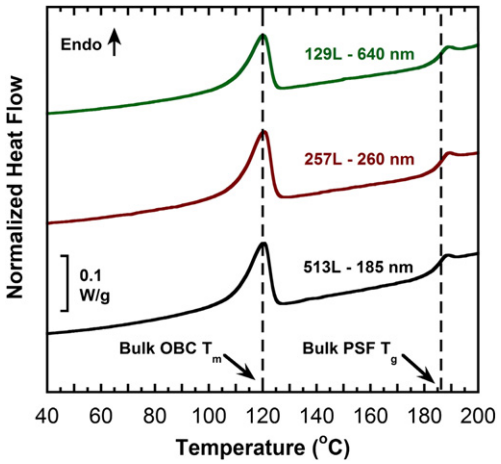

Fig. 3. Normalized DSC scans of PSF/OBC films (from 2nd heating at 10 °C/min) [25]. Each thermogram is labeled with the number of layers and the average PSF layer thickness. Dashed lines show the bulk values for the melting point of OBC and the T_g of PSF. Thermograms are offset vertically for easier viewing.

2.4. Differential scanning calorimetry (DSC)

A PerkinElmer DSC 6000 equipped with an Intracooler 6P was used throughout this study. A three-point temperature calibration using indium, tin, and zinc was performed prior to study. The heat flow calibration was performed using indium. The melting

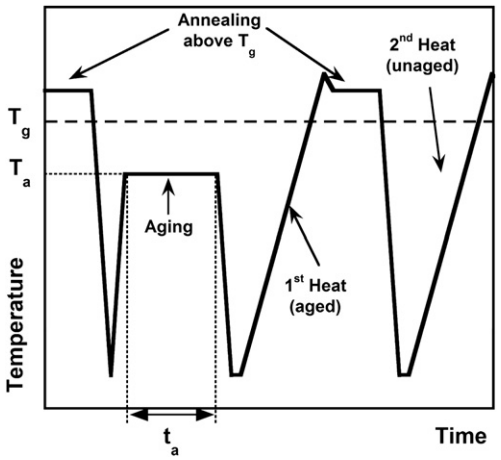

Fig. 4. General temperature program used in DSC aging studies. In this work, the aging temperature (T_a) was 170 °C, and the aging time (t_a) ranged from 5 to 600 min.

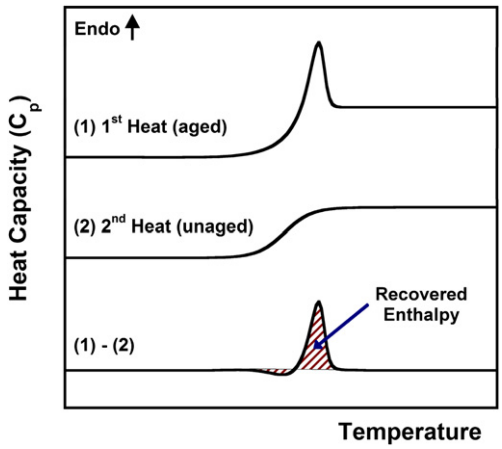

Fig. 5. Schematic drawing showing how ΔH is determined from heat capacity curves. Recovered enthalpy is calculated from DSC thermograms using the DSC software.

temperature and heat of fusion of indium were measured periodically to ensure that the instrument remained in calibration. All heating scans (including the calibration scans) were performed at a heating rate of 10 °C/min. The total mass of sample in the DSC pan was typically ~10–12 mg. The DSC thermograms (2nd heating) for the unaged PSF/OBC films are shown in Fig. 3. In these films, the T_g of PSF and the melting point of the OBC material in the layered films are the same as those in bulk (i.e., thick) samples. Because the PSF layers in these films have the same T_g as bulk PSF, aging at any particular temperature T_a will always be at the same value of T_g–T_a for both layered and bulk films.

2.5. Isothermal aging experiments

Isothermal aging experiments were performed at 170 °C (~16 °C below the PSF T_g). This temperature was chosen because it is outside the PSF glass transition region but still high enough to produce readily measurable changes in recovered enthalpy over time. Fig. 4 shows the temperature program used in the isothermal aging studies. The samples are annealed above the PSF T_g at 195 °C for 5 min, cooled at 40 °C/min through the transition region to 110 °C, and then immediately reheated at 40 °C/min to the aging temperature of 170 °C. They were then aged for a period of time, t_a, ranging from 5 to 600 min. A first heating scan from 110 °C to 200 °C at 10 °C/min was performed after cooling from the aging temperature to 110 °C and holding for 1 min to stabilize the DSC signal. A second heating scan, used as a reference scan, was performed after the first. For this scan, the sample was held at 195 °C for 5 min, cooled at 40 °C/min to 110 °C, held for 1 min, then heated at 10 °C/min to 200 °C. For each type of film (i.e., bulk, 129 layers, 257 layers, or 513 layers), the same sample was used to obtain the recovered enthalpy data at each aging time to eliminate possible sample-to-sample variation. The annealing temperature and upper limit for the scan temperature (200 °C) were chosen to minimize the possibility of layer breakup occurring during the experiment [49].

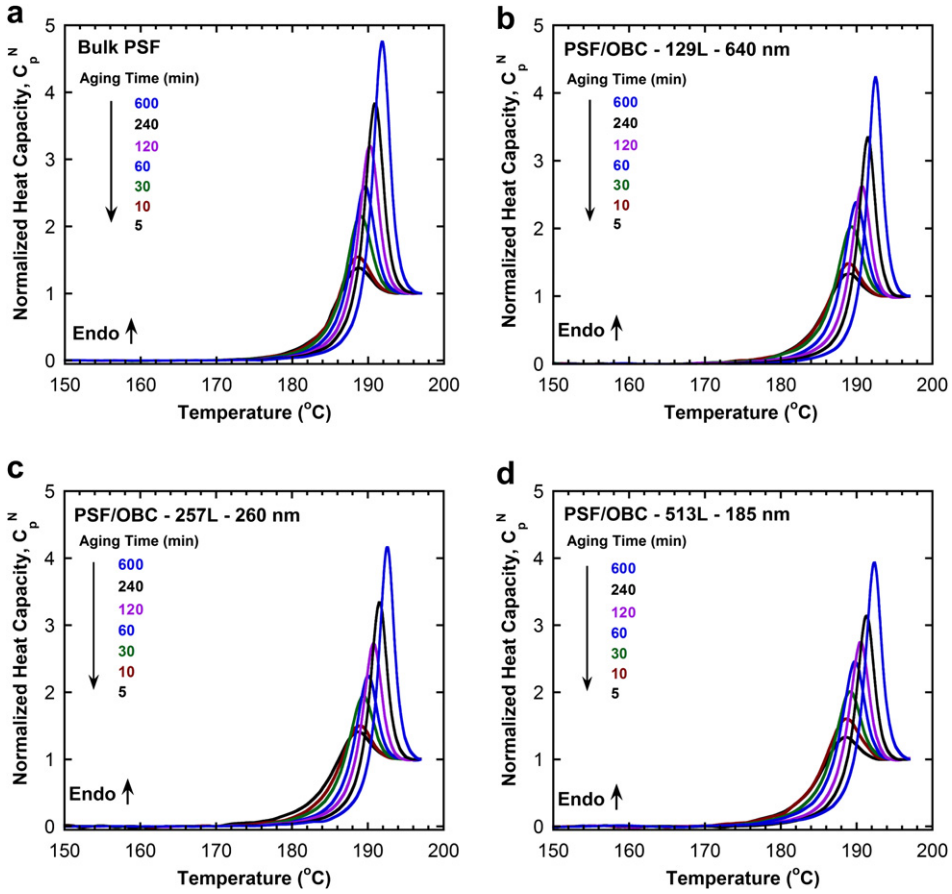

Fig. 6. Normalized heat capacity curves as a function of aging time for bulk PSF and multilayered PSF/OBC films aged at 170 °C. (a) Bulk PSF (b) 129-layer PSF/OBC (~640 nm PSF layers) (c) 257-layer PSF/OBC (~260 nm PSF layers) (d) 513-layer PSF/OBC (~185 nm PSF layers).

2.6. Cooling rate experiments

Experiments were performed to assess the dependence of structural relaxation on cooling rate in bulk and multilayered films. The glass transition temperature depends on the imposed cooling rate, and T_g values decrease with decreasing cooling rate [50,51]. The limiting fictive temperature (T_f') can be calculated from DSC heating scans of a sample immediately reheated after cooling at a desired rate. T_f' is dependent only on the cooling rate and can be used to approximate the T_g that would be measured on cooling at the same rate [52]. Badrinarayanan et al. studied the relationship between T_f' and T_g and found that T_f' is typically only ~1 °C lower than the T_g measured on cooling [53]. The value of T_f' after cooling from above T_g at a particular rate gives an indication of how much relaxation occurs during the cooling step, with samples that undergo more relaxation showing a lower value of T_f'. In these experiments, samples were cooled from 205 °C to 130 °C at rates ranging from 20 °C/min to 0.1 °C/min. For the slowest cooling rates (0.1, 0.2, and 0.5 °C/min), the samples were cooled to 150 °C at the prescribed rate and then cooled at 20 °C/min to the scan temperature. Because nearly all the relaxation occurs in the glass transition region and at temperatures just below it, very little relaxation occurs during cooling from 150 °C to 130 °C. This two-step cooling procedure saves a considerable amount of time without noticeably affecting the results. The samples were then reheated at 10 °C/min through the transition region. T_f' was calculated using the DSC software. Data for cooling rate versus temperature can be used to calculate $\Delta h^*/R$, a parameter used in phenomenological models of aging and structural relaxation in glasses [4,54]. This parameter provides a measure of the sensitivity of the glass transition to changes in experimental timescale for a given material.

3. Results and discussion

3.1. Recovered enthalpy in layered and bulk films aged isothermally

The enthalpy that is recovered upon reheating an aged sample through T_g can be quantified using Eq. (1).

$$\Delta H(T_a, t_a) = \int_{T_0<T_g}^{T_1>T_g} \left(C_p^{\text{aged}}(T_a, t_a, T) - C_p^{\text{ref}}(T)\right) \mathrm{d}T \quad (1)$$

In Eqs. 1, T_0 and T_1 are temperatures below and above the T_g, respectively. C_p^{aged} is given by the DSC thermogram of the aged sample, and C_p^{ref} is given by the DSC thermogram for the second heating scan (i.e., "unaged"), which is performed immediately after annealing above T_g and then cooling to the starting scan temperature. Fig. 5 illustrates the procedure used to calculate the recovered enthalpy. These calculations are performed using the PerkinElmer Pyris DSC software supplied with the instrument. To compare the recovered enthalpy values of the layered and bulk films, the values calculated with the DSC software must be normalized by the mass fraction of PSF (ω_{PSF}) in each sample using Eq. (2).

$$\Delta H_{PSF} = \frac{\Delta H_{\text{layered, total}}}{\omega_{PSF}} \quad (2)$$

By normalizing the recovered enthalpy values so that they have units of J/(g *PSF*), meaningful comparisons can be made between the aging responses of bulk and layered samples. Fig. 6(a–d) shows the normalized heat capacity curves for bulk and layered PSF samples aged between 5 and 600 min. In Fig. 6(a–d), longer aging times lead to greater peak heights, as expected. Normalization of the DSC curves is done to facilitate comparison between samples

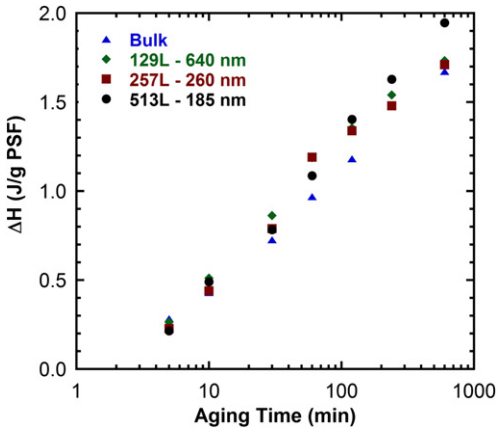

Fig. 7. Recovered enthalpy for bulk PSF and layered PSF/OBC films as a function of aging time at 170 °C. Recovered enthalpy values were calculated as shown in Fig. 5 and then divided by the mass fraction of PSF in the sample (determined via elemental analysis).

with different PSF content. The normalized heat capacity, C_p^N is calculated as follows:

$$C_p^N = \frac{C_p(T) - C_{pg}(T)}{\Delta C_p(T)} \quad (3)$$

In Eq. (3), $C_p(T)$ is the heat capacity given by the DSC scan, $C_{pg}(T)$ is the extrapolated glassy heat capacity, and $\Delta C_p(T)$ represents the difference between the extrapolated equilibrium liquid and glassy heat capacities at a given temperature. When defined this way, the value of C_p^N is 0 in the glassy region and equal to 1 in the equilibrium state above T_g. The normalized heat capacity curves for all samples are qualitatively similar, although the maximum value of C_p^N is greatest in the bulk sample. The calculation of C_p^N requires extrapolating a line representing the equilibrium state heat capacity, and because of the upper limit on temperature that is imposed to avoid possible layer breakup, this results in less data being available for the temperature regime above T_g. Thus, some uncertainty in the peak values of C_p^N is expected, especially for films aged for longer periods of time. Extrapolation of the equilibrium heat capacity line is not necessary for the calculation of recovered enthalpy. In their studies of stacked ultrathin polystyrene films, Koh

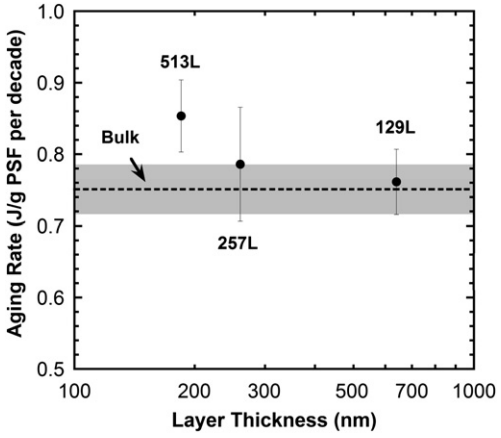

Fig. 8. Aging rates for bulk PSF and layered PSF/OBC films aged at 170 °C. The bulk value is shown as a dashed line. Errors bars are the uncertainties from fitting the recovered enthalpy data, and the uncertainty range for the bulk sample is indicated by the gray shaded area.

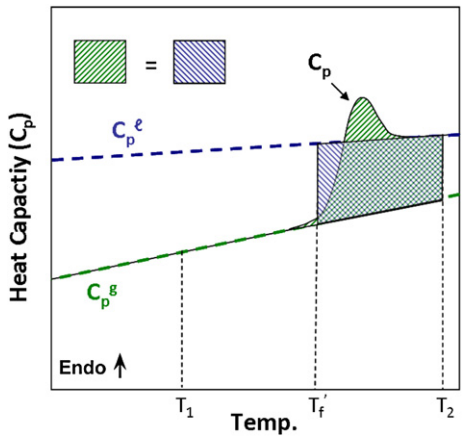

Fig. 9. Graphical explanation of the equal areas method for calculating the limiting fictive temperature from DSC thermograms (Eq. (5)).

and Simon observed that a 62 nm film showed a reduced peak value of C_p^N and a noticeably broader glass transition than a bulk film when the samples were aged 5° below T_g [9]. In this work, no apparent broadening of the glass transition was observed. Fig. 7 shows the calculated recovered enthalpy values as a function of aging time at 170 °C for the bulk and layered PSF samples. The calculated recovered enthalpy values at a given aging time and the rates of increase over time appear to be similar for the bulk and layered samples. To quantify the rates of increase, an aging rate for isothermal enthalpy relaxation can be defined as follows [16]:

$$r_{\Delta H} = \frac{d\Delta H}{d \log t} \tag{4}$$

When defined as such, the aging rate is simply the slope of the best-fit lines for the linear regions of the data sets shown in Fig. 7. A plot of the calculated aging rates as a function of layer thickness is shown in Fig. 8. The error bars in Fig. 8 represent the uncertainties in the slopes of the linear regression equations from Fig. 7. The 129-layer film (640 nm PSF layers) and the 257-layer film (260 nm PSF layers) have aging rates of 0.76 and 0.78 J/g per decade, respectively, which are similar to the bulk value of 0.75 J/g per decade. The calculated aging rate for a 513-layer film with ~185 nm PSF layers is 0.85 J/g per decade. Unfortunately, difficulties in extruding films with very thin continuous layers prevent us from studying PSF/OBC films with PSF layers that are significantly less than ~185 nm in thickness and assessing whether the apparent increase in aging rate with decreasing layer thickness continues as the PSF layers are made progressively thinner. Our previous DSC studies with layered films of PSF and an ethylene-1-octene copolymer (EO) aged at 170 °C revealed that for a film with ~180 nm PSF layers, the aging rate (as defined above) was 0.72 J/g per decade, which is similar to the bulk value of 0.75 J/g per decade reported here. More information about these studies and how they compare with the present work can be found in the Supplemental material. Based on the qualitative similarity between the DSC thermograms for the layered films, the similarity of the recovered enthalpy values for the layered and bulk films, and the findings of previous studies with PSF/EO films, we hesitate to assert that the aging of the 513-layer PSF/OBC film is truly accelerated relative to bulk. The PSF/OBC

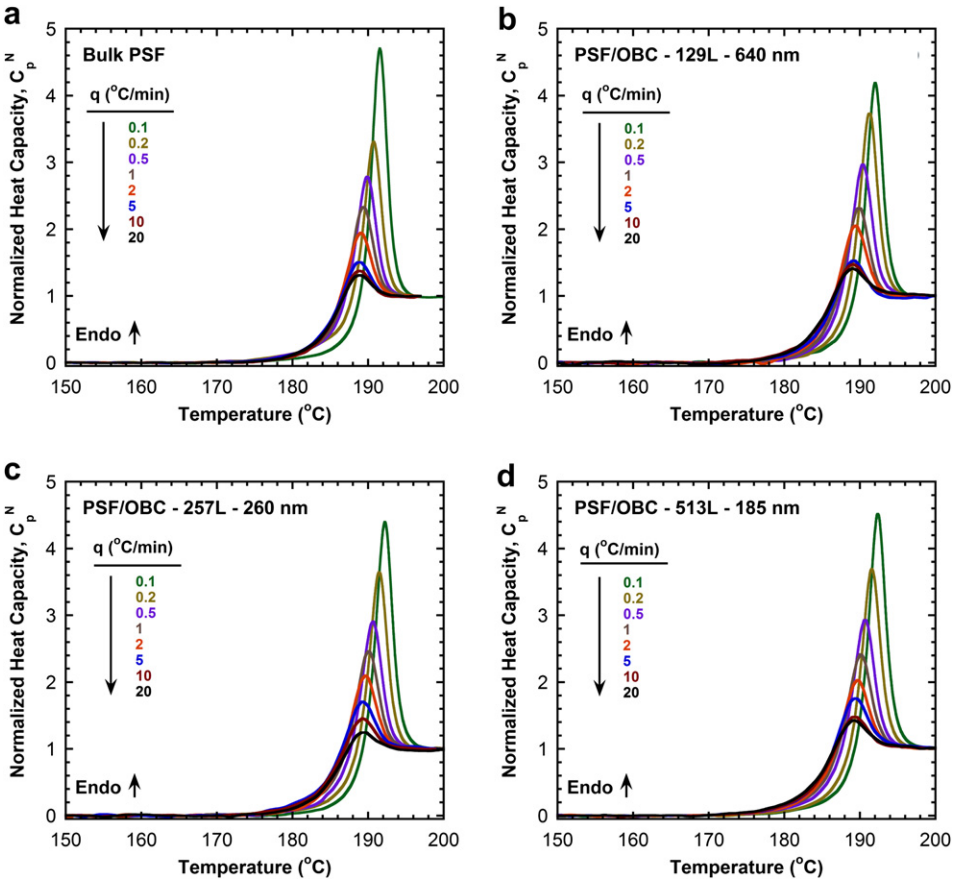

Fig. 10. Normalized heat capacity curves as a function of cooling rate for bulk PSF and multilayered PSF/OBC films (a) Bulk PSF (b) 129-layer PSF/OBC (~640 nm PSF layers) (c) 257-layer PSF/OBC (~260 nm PSF layers) (d) 513-layer PSF/OBC (~185 nm PSF layers).

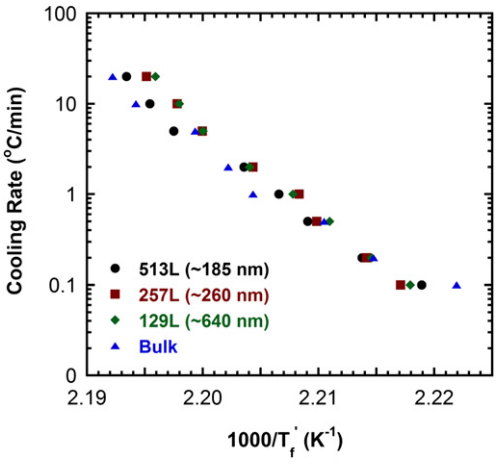

Fig. 11. Cooling rate dependence of the limiting fictive temperature (T_f') for bulk PSF and layered PSF/OBC films. Layer thickness is given in parentheses.

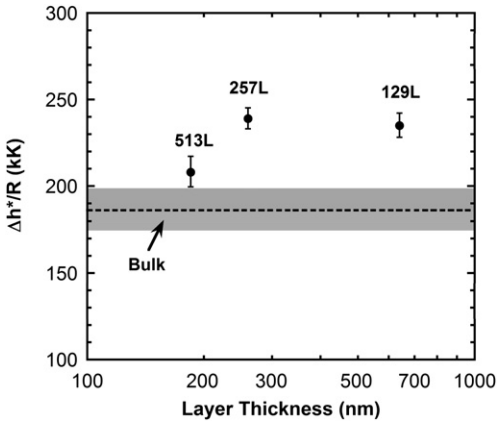

Fig. 12. Values of $\Delta h^*/R$ versus layer thickness for bulk PSF and layered PSF/OBC films. Values of $\Delta h^*/R$ were obtained using Eq. (6) and the data shown in Fig. 11. The error bars shown are the uncertainties from fitting the data of Fig. 11.

films are extruded at temperatures that allow for melt-state equilibration between PSF and OBC, resulting in well-adhered layers. The similarity between the aging of bulk and layered PSF films suggests that the nature of the interface has an important effect on aging behavior.

In a recent study by Langhe et al. of physical aging in multilayered PS/PC films using DSC, the aging rate in the PS layers systematically decreased with decreasing PS layer thickness when aged isothermally at 80 °C [16]. The decrease in aging rate was approximately linear with the logarithm of layer thickness. The differences in aging rate seen here (PSF layers aged at $T_g - 16$ °C) are less than those observed in the study by Langhe et al. (PS layers aged at $T_g - 24$ °C), and we did not observe a decrease in aging rate with decreasing layer thickness. Aside from the difference in both materials studied and aging temperature relative to T_g, another important difference between this work and the study of PS/PC layered films is that during aging of the PS layers, the confining PC layers are well below their T_g (PC $T_g \sim 145$ °C), whereas here the PSF layers are aged while the confining OBC layers are well above their T_g (OBC $T_g \sim -60$ °C). Thus, the PS layers in PS/PC films are confined by rigid, glassy PC ("hard" confinement), while the PSF layers in PSF/OBC films are confined by the rubbery, lower-modulus OBC material ("soft" confinement).

3.2. Calculation of T_f' and apparent activation enthalpy

The limiting fictive temperature of a glassy sample was calculated by the Pyris DSC software using the equal areas method of Moynihan [55,56]. A graphical illustration of this method is shown in Fig. 9. Two temperatures, T_1 and T_2, which are below and above the transition region, respectively, are chosen. The heat capacity lines for the equilibrium liquid (C_p^l) and glass (C_p^g) are extrapolated from the DSC thermogram for C_p, and T_f' is the value which satisfies the following equation:

$$\int_{T_1}^{T_2}\left(C_p - C_p^g\right)\mathrm{d}T = \int_{T_f'}^{T_2}\left(C_p^\ell - C_p^g\right)\mathrm{d}T \tag{5}$$

The Pyris DSC software is able to perform this calculation when supplied with T_1, T_2, and the extrapolated heat capacity lines. By measuring T_f' as a function of cooling rate (q), $\Delta h^*/R$ can be calculated using Eq. (6) [4].

$$\frac{\partial \ln|q|}{\partial\left(1/T_f'\right)} = -\frac{\Delta h^*}{R} \tag{6}$$

Fig. 10(a–d) shows the normalized heat capacity curves for bulk and layered PSF samples cooled at various rates and then reheated at 10 °C/min. Fig. 11 presents data for cooling rate versus $1000/T_f'$ that was used to determine $\Delta h^*/R$ for the layered and bulk PSF samples, and Table 3 shows the calculated $\Delta h^*/R$ values. A plot of these values is shown in Fig. 12. The value of $\Delta h^*/R$ for a bulk sample was 181 kK. The $\Delta h^*/R$ values of layered samples were higher than those of bulk PSF. The calculated values of $\Delta h^*/R$ did not exhibit any systematic dependence on layer thickness. In contrast, Koh and Simon observed that $\Delta h^*/R$ values decreased systematically with decreasing thickness in polystyrene films [9]. Lower values of T_f' (relative to bulk) were also observed for the thinner PS films, although this was primarily due to the thinner films having reduced T_g values. Langhe et al. studied the effect of cooling rate on

Table 3
Values of $\Delta h^*/R$ for bulk PSF and layered PSF/OBC films obtained from the data shown in Fig. 11.

Sample	PSF layer thickness	$\Delta h^*/R$
Bulk PSF	–	181 kK
129L	640 nm	233 kK
257L	260 nm	238 kK
513L	185 nm	206 kK

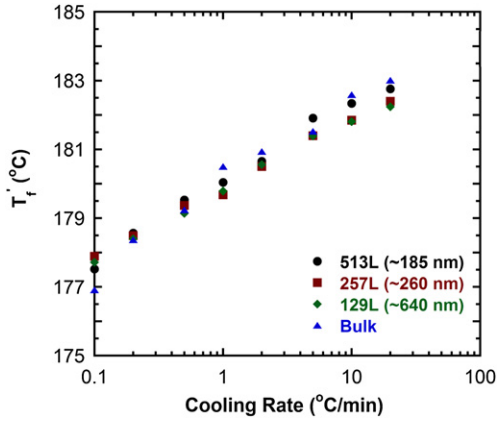

Fig. 13. Limiting fictive temperature (T_f') as a function of cooling rate for bulk PSF and layered PSF/OBC films.

recovered enthalpy in both bulk PS and layered PS/PC films [16]. In their study, the amount of enthalpy recovered upon reheating through the PS T_g was similar for all films and did not depend on layer thickness. Upon plotting our T_f' data versus the logarithm of the cooling rate (cf., Fig. 13), the absolute values of the fictive temperatures are within 1 °C for all samples at each cooling rate. Consequently, the amount of relaxation occurring during cooling is quite similar for all samples considered, which is largely in agreement with the findings of Langhe et al. in which no discernable impact of layer thickness on recovered enthalpy was observed for samples cooled at different rates.

4. Conclusions

Isothermal aging studies at 170 °C and cooling rate studies were performed on bulk PSF and multilayered PSF/OBC samples. The aging of thin PSF layers confined in these multilayered structures is largely similar to aging in bulk PSF for films for samples having PSF layer thicknesses of ~640 nm and ~260 nm. The film with 185 nm thick PSF layers showed a slightly higher aging rate than that of bulk PSF. Difficulties in preparing layered films with PSF layers thinner than ~185 nm prevented us from determining if the higher aging rate observed in the 513-layer film was truly due to decreasing film thickness. Cooling rate studies on layered PSF/OBC and bulk PSF films were also performed by varying the cooling rate through T_g and then measuring the limiting fictive temperature (T_f') of the samples upon reheating. T_f' was similar (within 1 °C) among all samples at each cooling rate. The results of the DSC studies presented here generally support the conclusions of our previous gas permeation aging studies of PSF/OBC and PSF/EO films aged at 35 °C, in which the aging rate was found to be independent of layer thickness and similar to the aging rate of bulk PSF. Freestanding thin films of PSF that have been previously studied using gas permeability tracking by Huang et al. [19,21] show highly accelerated aging relative to bulk and a strong dependence of aging rate on film thickness. The absence of a strong thickness dependence of the aging rates in multilayered PSF films when studied by DSC at temperatures close to T_g (170 °C) or by gas permeability tracking at temperatures far from T_g (35 °C) [25] tends to support the idea that accelerated aging in freestanding thin films relates to the presence of free surfaces (i.e., interfaces not in contact with, not adhering to, or only weakly interacting with a substrate). The multilayered films considered here and in our previous work are composed of PSF layers in intimate contact with rubbery confining layers and thus lack the large fraction of near-surface material that is present in freestanding films.

Acknowledgments

This research was supported by NSF Science and Technology Center for Layered Polymeric Systems (Grant DMR-0423914).

Appendix A. Supplementary material

Supplementary material associated with this article can be found, in the online version, at http://dx.doi.org/10.1016/j.polymer.2012.07.012.

References

[1] Struik LCE. Physical aging in amorphous polymers and other materials. Amsterdam: Elsevier; 1978.
[2] Hutchinson JM. Progress in Polymer Science 1995;20(4):703–60.
[3] Tool AQ. Journal of the American Ceramic Society 1946;29(9):240–53.
[4] Moynihan CT, Macedo PB, Montrose CJ, Gupta PK, DeBolt MA, Dill JF, et al. In: The glass transition and the nature of the glassy state, 279. Annals of the New York Academy of Sciences; 1976. p. 15–35.
[5] Narayanaswamy OS. Journal of the American Ceramic Society 1971;54(10):491–8.
[6] Hodge IM. Journal of Non-Crystalline Solids 1994;169(3):211–66.
[7] Petrie SEB. Journal of Polymer Science Part A-2: Polymer Physics 1972;10(7):1255–72.
[8] Marshall AS, Petrie SEB. Journal of Applied Physics 1975;46(10):4223.
[9] Koh YP, Simon SL. Journal of Polymer Science Part B: Polymer Physics 2008;46(24):2741–53.
[10] Boucher VM, Cangialosi D, Alegría A, Colmenero J, Pastoriza-Santos I, Liz-Marzan LM. Soft Matter 2011;7(7):3607.
[11] Cangialosi D, Boucher VM, Alegría A, Colmenero J. Polymer 2012;53(6):1362–72.
[12] Boucher VM, Cangialosi D, Alegría A, Colmenero J. Macromolecules 2010;43(18):7594–603.
[13] Lu H, Nutt S. Macromolecules 2003;36(11):4010–6.
[14] Flory AL, Ramanathan T, Brinson LC. Macromolecules 2010;43(9):4247–52.
[15] Simon SL, Park J-Y, McKenna GB. The European Physical Journal E – Soft Matter 2002;8(2):209–16.
[16] Langhe DS, Murphy TM, Shaver A, LaPorte C, Freeman BD, Paul DR, et al. Polymer 2012;53(9):1925–31.
[17] Huang Y, Wang X, Paul DR. Journal of Membrane Science 2006;277(1–2):219–29.
[18] Huang Y, Paul DR. Macromolecules 2005;38(24):10148–54.
[19] Huang Y, Paul DR. Polymer 2004;45(25):8377–93.
[20] Huang Y, Paul DR. Journal of Polymer Science Part B: Polymer Physics 2007;45(12):1390–8.
[21] Huang Y, Paul DR. Industrial & Engineering Chemistry Research 2007;46(8):2342–7.
[22] Huang Y, Paul DR. Journal of Membrane Science 2004;244(1–2):167–78.
[23] Cui L, Qiu W, Paul DR, Koros WJ. Polymer 2011;52(15):3374–80.
[24] Cui L, Qiu W, Paul DR, Koros WJ. Polymer 2011;52(24):5528–37.
[25] Murphy TM, Langhe DS, Ponting M, Baer E, Freeman BD, Paul DR. Polymer 2011;52(26):6117–25.
[26] McCaig MS, Paul DR. Polymer 1999;40(26):7209–25.
[27] McCaig M, Paul DR, Barlow JW. Polymer 2000;41(2):639–48.
[28] Priestley RD. Journal of Physics: Condensed Matter 2007;19(20):205120.
[29] Ellison CJ, Kim SD, Hall DB, Torkelson JM. The European Physical Journal E – Soft Matter 2002;8(2):155–66.
[30] Priestley RD, Broadbelt LJ, Torkelson JM. Macromolecules 2005;38(3):654–7.
[31] Priestley RD, Ellison CJ, Broadbelt LJ, Torkelson JM. Science 2005;309(5733):456–9.
[32] Labahn D, Mix R, Schönhals A. Physical Review E 2009;79(1):1–9.
[33] Fukao K, Miyamoto Y. Physical Review E 2000;61(2):1743–54.
[34] Fukao K, Sakamoto A. Physical Review E 2005;71(4):41803.
[35] Cangialosi D, Wübbenhorst M, Groenewold J, Mendes E, Picken SJ. Journal of Non-Crystalline Solids 2005;351(33–36):2605–10.
[36] Boucher VM, Cangialosi D, Alegría A, Colmenero J, González-Irun J, Liz-Marzan LM. Soft Matter 2010;6(14):3306.
[37] Cangialosi D, Wübbenhorst M, Groenewold J, Mendes E, Schut H, van Veen A, et al. Physical Review B 2004:70224213.
[38] Baker EA, Rittigstein P, Torkelson JM, Roth CB. Journal of Polymer Science Part B: Polymer Physics 2009;47(24):2509–19.
[39] Kawana S, Jones RAL. The European Physical Journal E – Soft Matter 2003;10(3):223–30.
[40] Pye JE, Rohald KA, Baker EA, Roth CB. Macromolecules 2010;43(19):8296–303.
[41] Huang Y, Paul DR. Macromolecules 2006;39(4):1554–9.
[42] Kim JH, Koros WJ, Paul DR. Polymer 2006;47(9):3104–11.
[43] Priestley RD. Soft Matter 2009;5(5):919–26.
[44] Pfromm PH, Koros WJ. Polymer 1995;36(12):2379–87.
[45] Rowe BW, Freeman BD, Paul DR. Polymer 2009;50(23):5565–75.
[46] Mueller CD, Nazarenko S, Ebeling T, Schuman TL, Hiltner A, Baer E. Polymer Engineering and Science 1997;37(2):355–62.
[47] Liu RYF, Bernal-Lara TE, Hiltner A, Baer E. Macromolecules 2004;37(18):6972–9.
[48] Schrenk W, Alfrey Jr T. Coextruded Multilayer polymer films and sheets. In: Paul D, Newman S, editors. Polymer blends, vol. 2. New York: Academic Press; 1978. p. 129–65.
[49] Jin Y, Hiltner A, Baer E. Journal of Polymer Science Part B: Polymer Physics 2007;45(10):1138–51.
[50] Hadac J, Slobodian P, Riha P, Saha P, Rychwalksi R, Emri I, et al. Journal of Non-Crystalline Solids 2007;353(28):2681–91.
[51] Moynihan CT, Easteal AJ, Wilder J, Tucker J. The Journal of Physical Chemistry 1974;78(26):2673–7.
[52] Moynihan CT. Phenomenology of the structural relaxation process and the glass transition. In: Seyler RJ, editor. Assignment of the glass transition. ASTM International; 1994. p. 32–49.
[53] Badrinarayanan P, Zheng W, Li Q, Simon SL. Journal of Non-Crystalline Solids 2007;353(26):2603–12.
[54] Hodge IM. Science 1995;267(5206):1945–7.
[55] Moynihan CT, Easteal AJ, DeBolt MA, Tucker J. Journal of the American Ceramic Society 1976;59(1–2):12–6.
[56] Debolt MA, Easteal AJ, Macedo PB, Moynihan CT. Journal of the American Ceramic Society 1976;59(1–2):16–21.